第 33 卷第 8 期
2017 年 8 月

无 机 化 学 学 报
CHINESE JOURNAL OF INORGANIC CHEMISTRY

Vol.33 No.8
1365-1373

可循环 SERS 基底 ZnO/Ag 纳米材料合成和表征

黄庆利*,[1,3] 李 靖[2] 魏文娴[3]

([1]徐州医科大学形态学科研实验中心,徐州 221004)

([2]徐州工程学院化学化工学院,徐州 221111)

([3]扬州大学测试中心,扬州 225009)

摘要:利用简易、绿色、一锅煮的水热法合成了花状氧化锌/银复合纳米材料。然后利用各种光谱和显微技术对复合物进行了表征,并讨论了其表面增强拉曼(SERS)性能和光催化性能。结果表明氢氧化钠的量对于这种复合纳米材料的形貌和性能具有重要的调节作用。和其他形貌的氧化锌/银复合纳米材料相比较,花状氧化锌/银复合纳米材料具有最佳的光催化性能。同时进一步以花状氧化锌/银复合纳米材料作为 SERS 基底研究其表面增强拉曼性能,结果表明这种复合材料同时具有很好的表面增强拉曼性能。光催化和表面增强拉曼结果表明这种花状氧化锌/银复合纳米材料有望在有机物检测中作为一种具有很好的可循环性的新表面增强拉曼基底材料。

关键词:纳米复合物;表面增强拉曼;电子显微镜;光催化;可循环

中图分类号:O614.12 **文献标识码**:A **文章编号**:1001-4861(2017)08-1365-09

DOI:10.11862/CJIC.2017.168

Synthesis and Characterization of ZnO/Ag Nanocomposites for Recyclable Surface-Enhanced Raman Scattering Substrate

HUANG Qing-Li*,[1,3] LI Jing[2] WEI Wen-Xian[3]

([1]*Research Facility Center for Morphology of Xuzhou Medical University, Xuzhou, Jiangsu* 221004, *China*)

([2]*School of Chemistry and Chemical Engineering, Xuzhou Institute of Technology, Xuzhou, Jiangsu* 221111, *China*)

([3]*Testing center, Yangzhou University, Yangzhou, Jiangsu* 225009, *China*)

Abstract: Multifunctional flower-like ZnO/Ag nanocomposites were prepared by a facile, green and one-pot hydrothermal method. The as-prepared samples were investigated by using various spectroscopic and microscopic techniques in detail. The surface-enhanced Raman scattering (SERS) performance and photocatalytic activity of the nanocomposites were also investigated. The results show that the amounts of NaOH play a key role in controlling the morphologies and properties of these nanocomposites. The flower-like ZnO/Ag nanocomposites exhibit the best photocatalytic performance for rhodamine 6G (R6G). Meanwhile, the optimized nanocomposites (the flower-like ZnO/Ag nanocomposites) are then employed to study the SERS performance, which also show excellent SERS activity. The photodegradation and SERS results reveal that ZnO/Ag nanocomposites act as promising candidates for a new substrate and exhibit high recyclability in the detection of organic molecules.

Keywords: Nanocomposites; surface-enhanced Raman scattering (SERS); electron microscopy; photocatalytic; recyclable

收稿日期:2017-03-12。收修改稿日期:2017-05-16。

国家自然科学基金(No.21505118)、江苏省自然科学基金(No.BK2150438)和徐州医科大学科研启动基金资助项目。

*通信联系人。E-mail:qlhuang@yzu.edu.cn,Tel:86-516-83262091,Fax:86-516-83262091

0 Introduction

With the rapid development of industry, an enormous amount of industrial dyes have brought serious threats to our health. Increasing attention has been paid to the detection and degradation of industrial dyes[1-6]. Surface-enhanced Raman scattering (SERS) has attracted tremendous attention and has been widely used as a powerful analytical tool [6-11]. Various approaches and techniques have been developed to fabricate SERS substrates in order to obtain sensitive and reproducible detection [12-16]. However, most of the standard SERS substrates were for one-time use only. And considering the valuableness of the noble metals, these SERS substrates cannot be completely explored as a routine analytical technique. Developing new-type multifunctional SERS substrates that not only provide real-time representation of information of the dyes, but also degrade them under light irradiation is of interest[17-34].

It is well known that semiconductors, due to their unique band structures, are quite appropriate photocatalyst materials. Considering the SERS performance of the noble metals, loading SERS-active noble metal nanoparticles onto semiconductor surface is a good way to design multifunctional platform[17-34]. It is possible to achieve both SERS and photocatalytic performances from a single semiconductor/metal nanocomposite. More advantageously, the photocatalytic performance of the semiconductor can be improved by loading of SERS-active metal nanoparticles onto semiconductor surface due to the reduction of the charge (electron-hole) recombination post-photon excitation[35-36]. And the SERS sensitivity was also enhanced due to the charge transfer (CT) between the semiconductor surfaces and the dyes[37].

Among these SERS-active noble metals, silver has been demonstrated as a good choice due to its low costs, high SERS enhancement and the ability to enhance photocatalytic activity of semiconductors. For semiconductors, ZnO is considered to be one of the suitable materials owing to its high photocatalytic activity, nontoxicity, biological inertness and chemical stability[38-39]. Moreover, ZnO can interact with metal particles and improve the SERS response. Therefore, Ag-ZnO nanocomposites boost great research interests[23-34]. Though various methods have been used to successfully synthesize the Ag/ZnO nanocrystal, it is necessary to develop time-saving and cost-effective methods to design Ag-ZnO nanocomposites with wide application.

In this work, a highly sensitive, reproducible and reusable Ag nanoparticle decorated ZnO SERS substrate was fabricated by a one-pot, facile hydrothermal method. The synthesis process is straightforward, simple, reproducible, cost effective and robust. Trace detection of R6G was studied based on ZnO/Ag nanocomposite as efficient surface enhanced Raman scattering platforms. The self-cleaning ability of the Ag/ZnO substrates was studied. High SERS and self-cleaning performances from a single ZnO/Ag nanocomposite could be achieved by adjusting its morphologies and composition. This study suggested that ZnO/Ag substrates with high SERS performance and self-cleaning property can serve as excellent substrates for multifunctional platform.

1 Experimetal

1.1 Materials

All the chemical reagents used in this work include silver nitrate ($AgNO_3$), sodium hydroxide (NaOH), zinc nitrate hexahydrate ($Zn(NO_3)_2\cdot 6H_2O$), PVP-30, rhodamine 6G (R6G), crystal violet (CV), congo red (CR) and ethanol (C_2H_5OH). All chemicals were analytically pure and were used as received without further purification. Deionized water was used throughout the experiment.

1.2 Synthesis of ZnO/Ag nanocomposites

Zinc nitrate hexahydrate ($Zn(NO_3)_2\cdot 6H_2O$, 6.0 mmol) was dissolved in mixed solution of 50 mL distilled water and 5 mL ethanol. Then 5 mL 0.05 $mol\cdot L^{-1}$ silver nitrate PVP-30 aqueous solution (the concentration of PVP-30 is 5.5 $g\cdot L^{-1}$) was added into the solution with stirring. After that, different amounts of NaOH (0.24 g, 0.48 g and 1.44 g) were added into the above solution. Finally the mixed solution was

transferred into a Teflon-lined autoclave of 80 mL capacity and was filled up to 85% of the total volume with deionized water. After being sealed and heated at 160 ℃ for 6 h, the autoclave was cooled to room temperature naturally. The resulting products were collected by centrifugation, washed with distilled water and ethanol for several times, and finally dried in vacuum at 70 ℃ for 12 h. The products were denoted as ZnO/Ag024, ZnO/Ag048 and ZnO/Ag144, respectively. To obtain pure ZnO flowers, a similar synthetic procedure was employed without silver nitrate solution, while other reaction conditions were kept the same as that of ZnO/Ag048.

1.3 Characterization

The phase purity of the products was characterized by X-ray diffraction (XRD, German Bruker AXSD8 ADVANCE X-ray diffractometer) using an X-ray diffractometer with Cu $K\alpha$ radiation (λ=0.154 18 nm). The scanning angle range (2θ) is from 20° to 80°. Corresponding working voltage and current were 40 kV and 40 mA respectively. Morphology information of the as-prepared nanoparticles was obtained on a Japan Hitachi S-4800 field emission scanning electron microscope (SEM) operated at accelerating voltage of 15 kV. Transmission electron microscope (TEM) images, high resolution transmission electron microscopy (HRTEM) images and elemental mapping images were obtained on an American FEI Tecnai G2 F30 S-TWIN field-emission transmission electron microscopy (operated at 300 kV). The ultraviolet-visible (UV-Vis) diffuse reflectance spectra were obtained on an America Varian Cary 5000 spectrophotometer. X-ray photoelectron spectra (XPS) were recorded on an ESCALAB 250Xi system (Thermo Scientific). Raman and surface-enhanced Raman scattering (SERS) spectra were measured using a Britain Renishaw Invia Raman spectrometer with a solid-state laser (excitation at 532 nm) at room temperature. The SERS and self-cleaning process were preformed on the glass where the dyes and the as-prepared samples were mixed. The self-cleaning process was preformed on the above glass under the irradiation by a 1 000 W Xe lamp for 40 min.

1.4 Photocatalytic measurement

A mixture of 10 mg ZnO/Ag composites and 100 mL 10^{-5} mol·L^{-1} R6G aqueous solution were put in bottle with a capacity of 200 mL. Prior to illumination, the suspensions were magnetically stirred in the dark for 30 min to ensure the establishment of absorption equilibrium of R6G on the sample surfaces. Subsequently, the suspension was irradiated under a 1 000 W Xe lamp (λ_{max}=532 nm), which was positioned about 10 cm away from the breaker. After a given irradiation time, about 3 mL the mixture was withdrawn and immediately centrifuged. The photocatalytic degradation process of R6G was monitored by measuring its absorption with a UV-Vis spectrophotometer.

2 Results and discussion

The XRD patterns of the as-prepared samples are shown in Fig.1. From the XRD patterns, it can be seen that all the diffraction peaks at 31.6°, 34.3°, 36.3°, 47.5°, 56.7°, 62.3°, 67.8° and 69.1° were observed in all patterns, which can be indexed to wurtzite ZnO (PDF No.36-1451). Besides, for ZnO-Ag nanocomposites, the diffraction peaks at 38.1°, 44.4° and 64.3° corresponding to Ag (PDF No.04-0783) were found. No peaks corresponding to other Ag-containing or Zn-containing phases were detected, which indicated that the ZnO/Ag nanocomposites were prepared by using one-pot hydrothermal reaction.

In this synthetic process, the amount of NaOH played a key role to determine the morphologies of

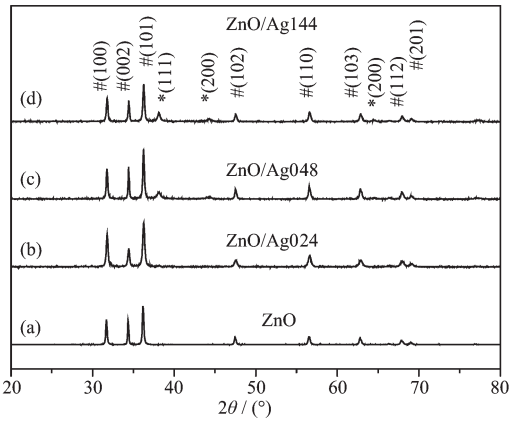

Fig.1　XRD patterns of ZnO and ZnO/Ag nanocomposites

ZnO/Ag nanocomposites. The morphologies of the typical flower-like ZnO and ZnO/Ag were found by scanning electron microscopy (SEM), as shown in Fig. 2. The SEM image of pure flower-like ZnO was shown in Fig.2a. It can be found that pure ZnO is made up of three-dimension (3D) flower-like hierarchical structures with good monodispersity, and the diameter of which is about 2 μm. Those flower-like architectures were assembled from a lot of nanoplates (Thickness: ~80 nm). ZnO/Ag nanocomposites with different morphologies were obtained when the amounts of NaOH were changed. The typical SEM images of these nanocomposites were shown in Fig.2b ~d. Only irregular particles were observed when the amount of NaOH was 0.24 g. Accompanying with the increasing of NaOH (0.48 g), uniform three-dimension (3D) flower-like hierarchical structures assembled from nanoplates were obtained. Many nanoparticles with the sizes of about 20 nm decorating uniformly on the surfaces of the ZnO nanoplates were found. Compared with those of pure flower-like ZnO, the surfaces became coarse. Further increasing the amount of NaOH to 1.44 g, sea urchin-like structures assembled from nanorods were found. However, the Ag nanopartcles attached on the surface of nanorods tend to agglomerate, which is unfavorable to improve the performance.

In order to investigate the structural details of the flower-like ZnO/Ag nanocomposites, the TEM, HRTEM and EDS mapping images were obtained. Fig. 3a and 3b further confirmed that the flower-like structures were constructed from Ag nanoparticles and ZnO nanoplates. HRTEM image (Fig.3c) displayed clear lattice fringes of the ZnO nanoplates and Ag nanopartilces. The interplanar distance of 0.26 nm corresponds to (002) crystal plane of ZnO, and that of 0.23 nm in the attached nanoparticle corresponds to Ag (111) crystal plane. Fig.3d shows the EDS elemental mappings of the nanocomposites. The different color images indicate Zn-, O-, Ag-enriched areas of the sample respectively, which confirms the composition of the nanocompistes.

XPS spectra were also investigated with the

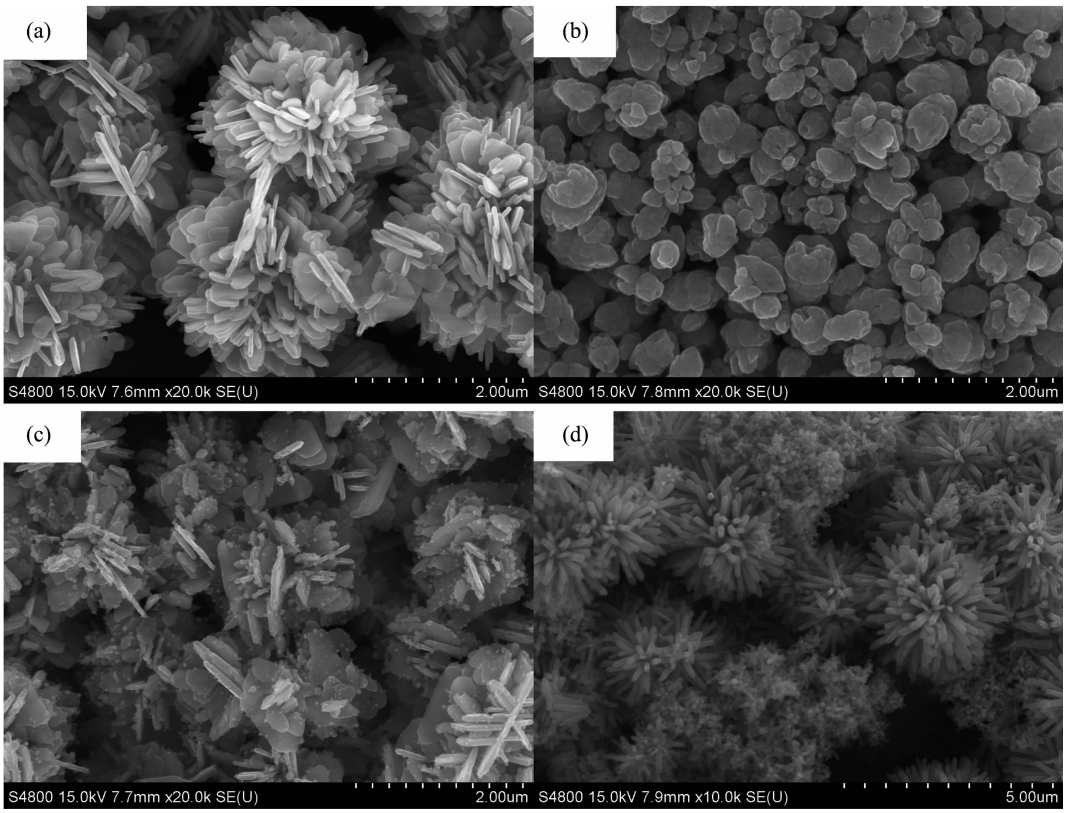

Fig.2 SEM images of pure flower-like ZnO (a), irregular ZnO/Ag nanocomposites (b), flower-like ZnO/Ag nanocomposites (c) and sea urchin-like ZnO/Ag nanocomposites (d)

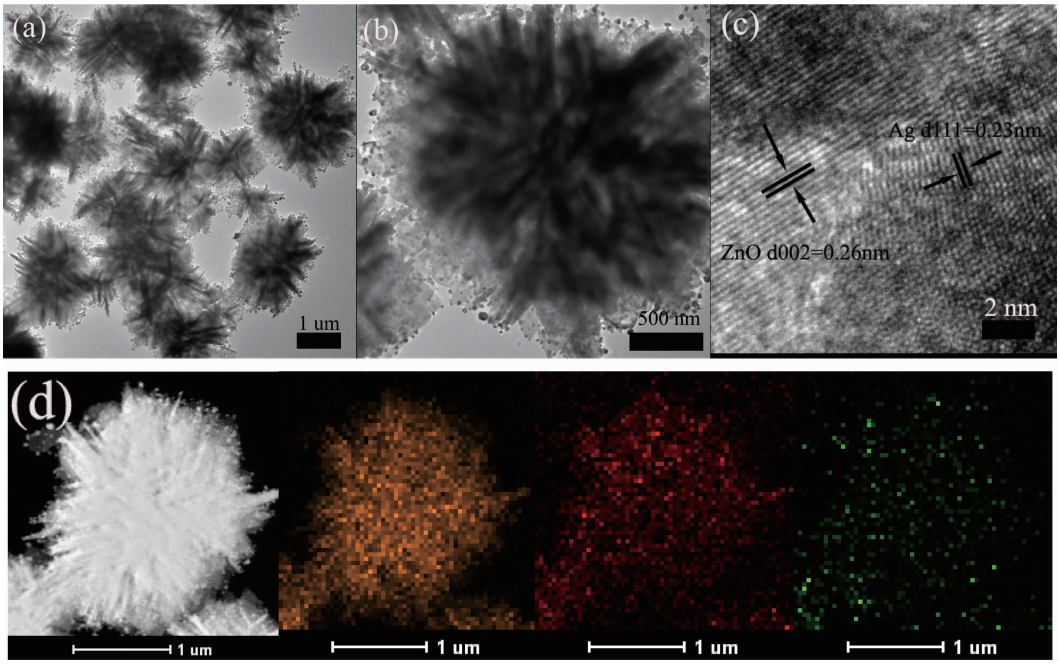

Fig.3　TEM (a, b), HRTEM (c) and EDS (d) mapping images of flower-like ZnO/Ag nanocomposites

binding energies calibrated using C1*s* (284.8 eV), as shown in Fig.4. For pure ZnO, the peaks Zn, O and C were found in Fig.4a. The presence of C is mainly from pump oil due to vacuum treatment before the XPS test. In comparison, for ZnO/Ag nanocomposites, the peaks of Zn, O and Ag can be clearly observed in Fig.4b, which are in good agreement with XRD as described above. Fig.4c shows high-resolution spectrum taken from the Ag region of the flower-like Ag/ZnO nanocomposites. Two characteristic peaks centered at 367.5 and 373.5 eV can be attributed to Ag3$d_{5/2}$ and Ag3$d_{3/2}$, respectively. There is a shift to the lower binding energy relative to the corresponding values of bulk Ag (Ag3$d_{5/2}$, 368.2 eV; Ag3$d_{3/2}$, 374.2 eV), which may be explained by electron transfer from metallic Ag to ZnO crystals at the interfaces of Ag/

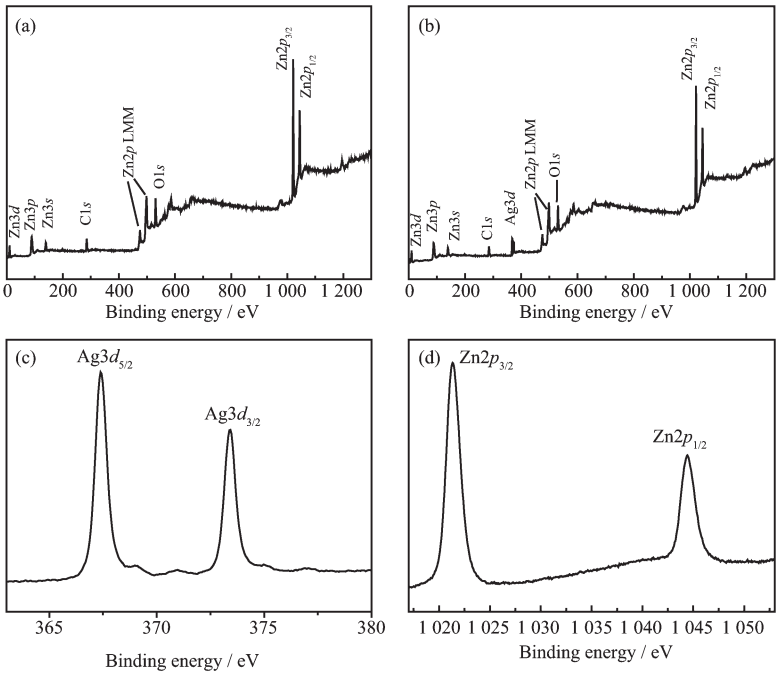

Fig.4　XPS spectra of pure ZnO flowers (a) and flower-like ZnO/Ag nanocomposites (b~d)

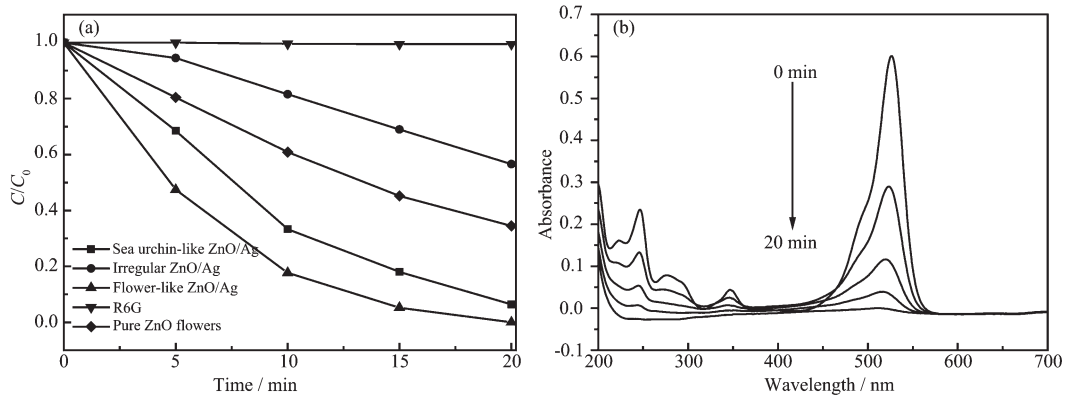

Fig.5 (a) Photocatalytic degradation of R6G with various samples under visible light irradiation in 20 min; (b) UV-visible spectrum of R6G under visible light irradiation using flower-like ZnO/Ag nanocomposites in 20 min

ZnO nanocomposites based on different Fermi levels of two components. In Fig.4d, two strong peaks center on 1 021.3 and 1 044.3 eV, which are in agreement with the binding energies of Zn2$p_{3/2}$ and Zn2$p_{1/2}$, respectively. Therefore, the XPS result further confirmed the sample is composed of ZnO and Ag.

Metal-decorated semiconductor nanoparticles are well known for their photocatalytic activity. Fig.5a showed the plots for the R6G concentration ratio (C/C_0) as a function of irradiation time over ZnO/Ag nanocomposites and pure ZnO flowers under the same condition. The R6G was quickly degraded completely in 20 minutes with flower-like ZnO/Ag nanocomposites as catalyst. While with the same catalytic time, the degradation rate with pure ZnO flowers as catalyst was only 65.5%. And R6G conversion over irregular ZnO/Ag nanocomposites and sea urchin-lie ZnO/Ag nanocomposites was 43.4% and 93.6%, respectively. It is clear that flower-like ZnO/Ag nanocomposites show the best performance. The changes of UV-Vis absorption spectra of R6G over flower-like ZnO/Ag nanocomposites were also shown in Fig.5b. The reaction under visible light irradiation resulted in a transparent solution after 20 min due to the destruction of the chromophoric structures of R6G.

The optical absorption property of the as-prepared samples, which is relevant to the electronic structure feature, is tested to explain the change in photocatalytic activity. The diffuse reflectance spectra of the as-prepared samples were demonstrated in Fig. 6. It can be clearly seen that absorption at about 375 nm was found in all curve, which is assigned to the absorption of ZnO semiconductor. For ZnO/Ag nanocomposites, new absorbance peaks at about 419, 436, 442 nm were observed in visible region in irregular ZnO/Ag, flower-like ZnO/Ag and sea urchin-like ZnO/Ag nanocomposites, respectively, which is attributed to the characteristic band of the plasma of Ag nanoparticles on the surface of these samples. It is clear that ZnO flowers before Ag nanoparticles deposition can only absorb UV light with wavelengths shorter than 400 nm because the band-band electron transition of the ZnO. After Ag nanoparticles deposition, ZnO/Ag nanocomposites exhibited enhanced capability to absorb visible light between 400 and 800 nm. Therefore, the ZnO/Ag nanocomposites can be readily excited by visible light, which could produce electron-hole pairs and subsequently enhance the

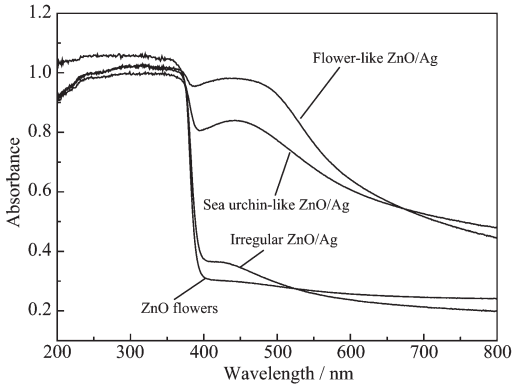

Fig.6 DRS spectra of the ZnO flowers and ZnO/Ag nanocomposites

photocatalytic performance.

Fig.7a shows the SERS spectra using flower-like ZnO/Ag nanocomposites as substrate for different concentrations of R6G. It can be seen that the featured bands of R6G molecules are clearly identified [40]. The bands at 1 362, 1 510, and 1 650 cm^{-1} originate from the aromatic stretching vibrations. Peaks at 770 and 1 130 cm^{-1} are assigned to the out-of-plane and in-plane bending vibrations of C-H, respectively. The peak at 612 cm^{-1} is associated with the in-plane bending vibration of C-C-C ring. As the concentration of R6G decreased, the spectral intensities became quite weak. Under our experimental conditions, the detection limit of R6G was estimated to be around 1 nmol·L^{-1}. To further assess flower-like ZnO/Ag nanocomposites SERS substrates, the SERS spectra of R6G were obtained on bare glass substrate and pure ZnO flowers substrates. Fig.7b and 7c depict the Raman spectra of R6G molecules taken from glass substrates and pure ZnO flower substrates, respectively. No peak of R6G was detected when commercial glass was used SERS substrate in Fig.7b. Very weak peaks were found when ZnO flowers were used SERS substrate in Fig. 7c. The average enhancement factors (EF) were estimated according to our early report[41]. The value of EF was approximately estimated to be in the order of 10^6, indicating that the flower-like ZnO/Ag nanocomposite SERS substrate was highly sensitive and it was sufficient enough to directly observe a trace amount of organic dyes.

The reproducibility of the substrate is an important factor for SERS detection. The reproducibility of flower-like ZnO/Ag nanocomposite substrate was examined with the SERS spectra taken from randomly selected 10 positions on the substrates. As shown in Fig.8a, the Raman spectra taken at different positions were nearly same. Fig.8b depicts the SERS signal of R6G in an intensity-laser spot at 1 650 cm^{-1}. The relative standard deviation (RSD) of

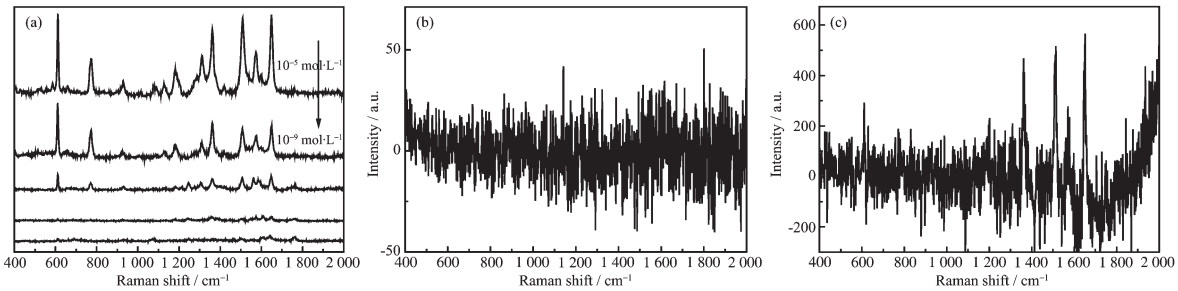

Fig.7 (a) SERS spectra of different concentrations of R6G absorbed on the flower-like ZnO/Ag nanocomposites; (b) Raman spectra of R6G (10^{-5} mol·L^{-1}) absorbed on bare glass; (c) SERS spectra of R6G (10^{-5} mol·L^{-1}) absorbed on the pure ZnO flowers

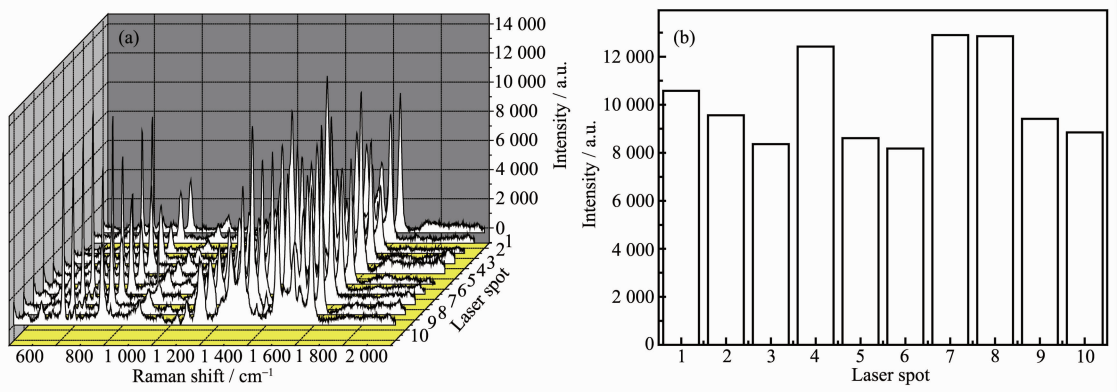

Fig.8 (a) SERS spectra of R6G taken from randomly selected 10 positions on the flower-like ZnO/Ag nanocomposites; (b) Corresponding SERS signal intensities of R6G for the bands of 1 650 cm^{-1} recorded at randomly selected 10 positions on the flower-like ZnO/Ag nanocomposites

SERS intensity for 10 different sites on flower-like ZnO/Ag nanocomposite was calculated. The RSD (12.6%) is less than 15.0%, which indicated that the flower-like SERS substrate had good reproducibility. A reasonable mechanism for the superior SERS performance may be attributed to the uniform distribution of Ag nanoparticles on the surface of ZnO nanoplates.

As is well known, the photocatalytic activity of ZnO/Ag could also be applied to remove adsorbed molecules under visible light due to its high absorption of visible light. The SERS recyclable applications of flower-like ZnO/Ag nanocomposite were examined. Fig.9 shows that the SERS signals are well reproduced after each visible light cleaning and R6G adsorption (10^{-5} mol·L^{-1}). No Raman signal of R6G molecules was detected anymore after 40 min irradiation of visible light, suggesting that the R6G molecules were degraded into small molecules such as CO_2 and H_2O. The residual R6G molecules on flower-like ZnO/Ag nanocomposite should be less than the detection limit. When R6G solution was doped on the SERS substrate and dried, the Raman signals emerged again. It can be found that flower-like ZnO/Ag nanocomposite had a good repeatability in the five cycles. Other dyes (CV and CR, 10^{-5} mol·L^{-1}) were also used to confirm the SERS performance of flower-like ZnO/Ag nanocomposite. It can be found that characteristic SERS spectra of these dyes (CV and CR) could be obtained from the same substrate in Fig. 10[41]. And no Raman signal of these dyes (CV and CR) was detected anymore after 40 min irradiation of visible light. This indicated that the flower-like ZnO/Ag nanocomposite acted as excellent SERS substrates exhibiting recyclability for reuse. The mechanism of the self-cleaning of the ZnO/Ag nanocomposite was also discussed. The excited electrons by visible light on the surface of Ag nanoparticles will move into the conduction band of ZnO through their interface. Then, superoxide radicals are produced when those electrons are captured by oxygen adsorbed on the surface of the nanocomposites. And the hydroxyl is formed due to interactions between the corresponding holes and the surface H_2O. Consequently, the organic dyes are degraded by these superoxide radicals and hydroxyl.

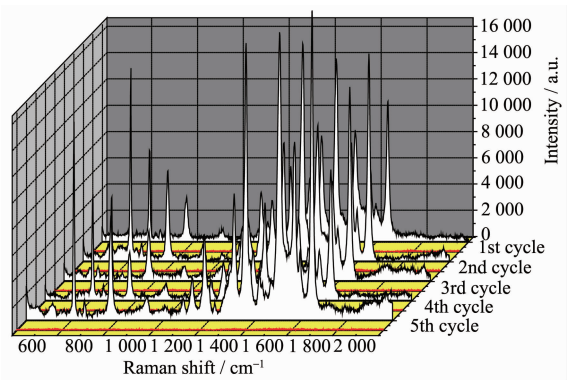

Fig.9 SERS spectra of R6G absorbed on flower-like ZnO/Ag nanocomposites and the repeating cleaning and recovery processes for five cycles

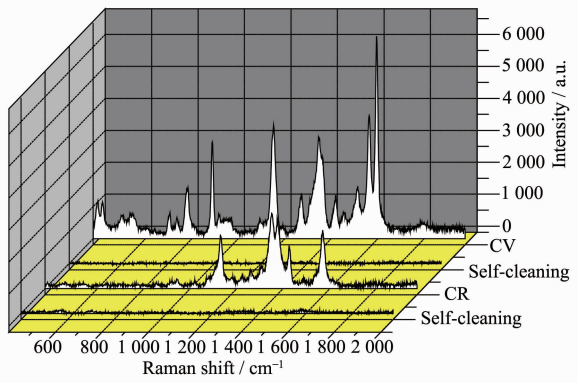

Fig.10 SERS spectra of other dyes (CV and CR, 10^{-5} mol·L^{-1}) absorbed on flower-like ZnO/Ag nanocomposites and their self-cleaning processes

3 Conclusions

In conclusion, as a multifunctional SERS active substrate, recyclable ZnO/Ag nanocomposite was prepared by a simple hydrothermal method. Experiments testified such flower-like ZnO/Ag nanocomposite to be a kind of excellent substrate for SERS-based sensitive molecular sensing. Meanwhile, target organic dyes can be degraded into clean inorganic molecules by visible-irradiation using this nanocomposite. This recyclable strategy opens a new opportunity in avoiding the single-use problem of traditional SERS substrates. This work exhibits a promising application for the detection of organic pollutants as online sensors capable of monitoring continuous reactions in real time.

References:

[1] Kaur J, Gupta K, Kumar V, et al. *Ceram. Int.*, **2016**,**42**:2378-2385

[2] WANG Yuan-You(王元有), GONG Ai-Qin(龚爱琴), YU Wen-Hua(余文华). *Chinese J. Inorg. Chem.*(无机化学学报), **2017**,**33**(3):509-518

[3] Wang H H, Peng D L, Chen T, et al. *Ceram. Int.*, **2016**,**42**:4406-4412

[4] Minioti K S, Sakellariou C F, Thomaidis N S. *Anal. Chim. Acta*, **2007**,**583**:103-110

[5] López-Montes A M, Dupont A-L, Desmazières B, et al. *Talanta*, **2013**,**114**:217-226

[6] MENG Wei(孟卫), ZHANG Ling-Yan(张玲艳), JIANG Xiao-Hong(江晓红), et al. *Chem. J. Chinese Universities*(高等学校化学学报), **2013**,**29**(3):571-576

[7] ZHAO Hong(赵红), FU Hong-Gang(付宏刚), TIAN Chun-Gui(田春贵), et al. *Chem. J. Chinese Universities*(高等学校化学学报), **2011**,**32**(10):2387-2390

[8] ZHANG Hao-Ran(张浩然), MAN Shi-Qing(满石清). *Chin. J. Anal. Chem.*(分析化学), **2011**,**39**(6):821-826

[9] López-López M, García-Ruiz C. *Trends Anal. Chem.*, **2014**, **54**:36-44

[10]Wang C, Gu H M, Lü M, et al. *Spectrochim. Acta Part A*, **2014**,**122**:65-74

[11]Hughes J, Izake E L, Lott W B, et al. *Talanta*, **2014**,**130**:20-25

[12]Jiang T, Wang B B, Zhang L, et al. *J. Alloys Compd.*, **2015**, **632**:140-146

[13]Gong X, Bao Y, Qiu C, et al. *Chem. Commun.*, **2012**,**48**:7003-7018

[14]Shiohara A, Wang Y S, Liz-Marzán L M. *J. Photochem. Photobiol. C*, **2014**,**21**:2-25

[15]Bian J C, Li Z, Chen Z D, et al. *Appl. Surf. Sci.*, **2011**,**258**:1831-1835

[16]ZHOU Xin(周鑫), YAO Ai-Hua(姚爱华), ZHOU Tian(周田), et al. *Chem. J. Chinese Universities*(高等学校化学学报), **2014**,**30**(3):543-549

[17]Du J, Jing C. *J. Phys. Chem. C*, **2011**,**115**:17829-17835

[18]Dong L H, Zhu J Y, Xia G Q. *Solid State Sci.*, **2014**,**38**:7-12

[19]Sun Y. *Adv. Funct. Mater.*, **2010**,**20**:3646-3657

[20]Yang L B, Li P, Liu J H. *RSC Adv.*, **2014**,**4**:49635-49646

[21]Fang H, Zhang C X, Liu L, et al. *Biosens. Bioelectron.*, **2015**,**64**:434-441

[22]Yang L B, Jiang X, Ruan W D, et al. *J. Phys. Chem. C*, **2009**,**113**:16226-16231

[23]Li Z J, Zhu K X, Zhao Q, et al. *Appl. Surf. Sci.*, **2016**,**377**:23-29

[24]Chen C, Zhou X, Ding T T, et al. *Mater. Lett.*, **2016**,**165**:55-58

[25]Koleva M E, Nedyalkov N N, Atanasov P A, et al. *J. Alloys Compd.*, **2016**,**665**:282-287

[26]Milekhin A, Sveshnikova L, Duda T, et al. *Physica E*, **2016**, **75**:210-222

[27]Jayram N D, Sonia S, Poongodi S, et al. *Appl. Surf. Sci.*, **2015**,**355**:969-977

[28]He X, Wang H, Li Z B, et al. *Nanoscale*, **2015**,**7**:8619-8626

[29]Li R, Han C, Chen Q W. *RSC Adv.*, **2013**,**3**:11715-11722

[30]Cui S Y, Dai Z G, Tian Q Y, et al. *J. Mater. Chem. C*, **2016**,**4**:6371-6379

[31]He X, Wang H, Li Z B, et al. *Phys. Chem. Chem. Phys.*, **2014**,**16**:14706-14712

[32]Zhao K Y, Lin J, Guo L. *RSC Adv.*, **2015**,**5**:53524-53528

[33]Hao R, Lin J, Wang H, et al. *Phys. Chem. Chem. Phys.*, **2015**,**17**:20840-20845

[34]Zang Y S, Yin J, He X, et al. *J. Mater. Chem. A*, **2014**,**2**:7747-7753

[35]Chai B, Wang X, Cheng S Q, et al. *Ceram. Int.*, **2014**,**40**:429-435

[36]Zhang D, Li J, Chen Y, et al. *CrystEngComm*, **2012**,**14**:6738-6743

[37]Kandjani A E, Mohammadtaheri M, Thakkar A, et al. *J. Colloid Interface Sci.*, **2014**,**436**:251-257

[38]LI Li(李丽), LIU Xiao-Ming(刘晓明), ZHOU Shu-Ting(周舒婷), et al. *Chinese J. Inorg. Chem.*(无机化学学报), **2016**,**32**(2):241-249

[39]WANG Xin-Juan (王新娟), XIAO Yang(肖洋), XU Fei(徐斐), et al. *Chinese J. Inorg. Chem.*(无机化学学报), **2014**,**30**(8):1821-1826

[40]Huang Q L, Zhu X S. *Talanta*, **2013**,**105**:117-123

[41]Huang Q L, Wang J M, Wei W X, et al. *J. Hazard. Mater.*, **2015**,**283**:123-130